Published in final edited form as:
J Nanosci Nanotechnol. 2011 February ; 11(2): 919–928. doi:10.1166/jnn.2011.3536.

Modeling Particle Shape-Dependent Dynamics in Nanomedicine

Samar Shah[1], **Yaling Liu**[2,*], **Walter Hu**[3], and **Jinming Gao**[4]

[1] Department of Mechanical and Aerospace Engineering, The University of Texas at Arlington, Arlington, Texas, 76019

[2] Department of Mechanical Engineering and Mechanics, Bioengineering Program, Lehigh University, Bethlehem, PA 18015 USA

[3] Department of Electrical Engineering, The University of Texas at Dallas, Richardson, TX 75080

[4] Department of Pharmacology, Harold C. Simmons Comprehensive Cancer Center, University of Texas Southwestern Medical Center, Dallas, TX 75390

Abstract

One of the major challenges in nanomedicine is to improve nanoparticle cell selectivity and adhesion efficiency through designing functionalized nanoparticles of controlled sizes, shapes, and material compositions. Recent data on cylindrically shaped filomicelles are beginning to show that non-spherical particles remarkably improved the biological properties over spherical counterpart. Despite these exciting advances, non-spherical particles have not been widely used in nanomedicine applications due to the lack of fundamental understanding of shape effect on targeting efficiency. This paper intends to investigate the shape-dependent adhesion kinetics of non-spherical nanoparticles through computational modeling. The ligand-receptor binding kinetics is coupled with Brownian dynamics to study the dynamic delivery process of nanorods under various vascular flow conditions. The influences of nanoparticle shape, ligand density, and shear rate on adhesion probability are studied. Nanorods are observed to contact and adhere to the wall much easier than their spherical counterparts under the same configuration due to their tumbling motion. The binding probability of a nanorod under a shear rate of 8 s^{-1} is found to be three times higher than that of a nanosphere with the same volume. The particle binding probability decreases with increased flow shear rate and channel height. The Brownian motion is found to largely enhance nanoparticle binding. Results from this study contribute to the fundamental understanding and knowledge on how particle shape affects the transport and targeting efficiency of nanocarriers, which will provide mechanistic insights on the design of shape-specific nanomedicine for targeted drug delivery applications.

Keywords

Adhesion kinetics; Brownian dynamics; Immersed finite element method; nanorod; nanomedicine

I. Introduction

In recent years, nanoparticulate systems have been widely used for diagnostic imaging and targeted therapeutic applications[1–9]. Various nanoplatforms, including liposomes[10,11], polymeric micelles[12–14], quantum dots[15,16], Au/Si/polymer shells[17–19], and dentrimers[20–22] have been established with distinctive chemical compositions and biological properties. Extensive studies have elucidated the effects of particle *size* (mostly

*Corresponding author. Tel.: +1-610-758-5839; fax: +1-610-758-6224. yal310@lehigh.edu (Y. Liu).

from spherical ones) on their clearance, circulation, extravasation, and distribution *in vivo*. However, the effects of particle *shape* on its fate are much less understood in nanomedicine. In nature, viruses have a variety of shapes from icosahedral to bullet/rod, yet the biological functions of shape are not clearly understood in relation to host infection and virus survival. Recently, synthetic non-spherical nanoparticles have shown significantly improved biological properties over their spherical counterparts. For example, cylindrically shaped filomicelles can effectively evade the non-specific uptake by the reticuloendothelial systems and persist in the circulation up to one week after intravenous injection (~10 times longer than the spheres)[23]. Dai and coworkers reported that single-walled carbon nanotubes (SWNT, diameter 1–5 nm, length 100–300 nm) can enhance polyvalent targeting of surface-bound peptide to the tumor cells, leading to highly elevated particle accumulation (13% injected dose/g tissue as compared to 1–2% for spherical particles) in tumors[24]. Sailor and coworkers demonstrated improved tumor accumulation and retention of worm-shaped iron oxide nanoparticles that are encoded with F3 peptides over spherical counterparts[25]. Despite these exciting advances, a fundamental understanding of the impact of shape in biological systems is still lacking.

The targeted delivery process involves interplay of particle transport, hydrodynamic force, and multivalent interactions with targeted biosurfaces[26]. Due to the small size of nanoparticles and the dynamic nature of the transportation-deposition process, it is a very challenging task to explore this phenomenon experimentally. Theoretical works of nanoparticle deposition are limited to simple spherical or oblate shape under an ideal configuration and steady state condition[27–29]. Theoretical modeling of nanoparticle adhesion kinetics has focused mostly on spherical nanoparticles. It is only recently that non-spherical nanoparticle attracted some attention. Winter et. al.[30] and Liu et. al.[31,32] have performed numerical simulations of dielectrophoresis of non-spherical particles. Decuzzi and Ferrari[27–29] have studied the margination of nanoparticle vectors in blood stream, where the nanoparticles diffusion in a Newtonian fluid was investigated. The same authors have also studied the adhesion probability of nanoparticles under an equilibrium configuration. In their work, the margination and adhesion process are studied separately. Djohari and Dormidontova[33] studied kinetics of spherical nanoparticle targeting to cell surface through dissipative particle dynamics. The shape of the adsorbed nanoparticle was found to become ellipsoidal with increasing binding energy. Janus-like nanoparticles with ligands coated on one side of the nanoparticle were observed to bind faster than that with uniformly coated ligands. Mody et. al.[34,35] studied platelet motion near a wall under shear flow and found that hydrodynamic force did affect platelet adhesion to wall surface. The same authors[34,35] also studied the influence of Brownian motion on platelet flow behavior and found that Brownian motion does not play an important role in influencing platelet-shaped cells at physiological shear rates. However, the size (~2 μm) and the shape (oblate) of the platelet is not comparable to that of nanoparticles and the behavior observed for platelet might not be applicable for nanoparticles. So far, only simple spherical or oblate-shaped nanoparticles are considered in literature, leaving rod and disk shaped nanoparticles un-explored. A coupled model that links margination with adhesion kinetics and applicable to nanoparticle of various shapes is yet to be developed. Thus, characterization of this process for arbitrarily shaped nanoparticle through a dynamic multiscale model is crucial to provide biological insights on the transportation and adhesion mechanisms.

This paper presents for the first time, the simulation result for dynamic transportation and adhesion of non-spherical nanoparticles to vascular wall under shear flow using Brownian dynamics method coupled with adhesion kinetics model through the Immersed Finite Element Method (IFEM) platform[36–41]. In the following sections of this paper, the nanoparticle adhesion kinetics theory and modeling method are described first. Then, adhesion processes and trajectories for nanoparticles of different shapes and ligand densities

are presented. Next, the binding probability of nanoparticles is studied for a range of channel thicknesses. Finally, the conclusion and future work are presented.

II. Nanoparticle Adhesion Kinetics

To achieve targeted drug delivery, nanoparticles are usually coated with polymers that bind specifically to a particular type of receptors on the vessel cell surface [42]. The ligand-receptor binding will be coupled with Brownian dynamics with the Immersed Finite Element (IFEM) platform. IFEM can be used for fully coupled fluid-structure interaction problems, i.e., solving particle motion in a fluid while capturing the influence of particle on fluid flow. However, due to Brownian motion, it is computationally expensive to calculate the change of fluid flow due to particle motion at every time step. Since the effect of nanoparticle motion is limited locally, we neglect the influence of particle motion on the fluid flow and focus on the particle motion and the adhesion process. Moreover, although IFEM can handle deformable particles immersed in a fluid, the nanoparticles are treated as rigid bodies in this work since our focus is on particle shape effect on adhesion process. The particle compliance will be the topic of future studies.

The ligand-receptor binding is described as a non-covalent interaction process. When a particle approaches the vascular wall, ligands on the particle surface form bonds with receptors on the vascular wall, as demonstrated in Fig. 1. An adhesion kinetic equation is used to calculate the bond density N_b [43]:

$$\frac{\partial N_b}{\partial t} = k_f(N_l - N_b)(N_r - N_b) - k_r N_b \tag{1}$$

Where, N_l and N_r are the ligand and receptor densities; k_r and k_f are the reverse and forward reaction rates, respectively. This interaction model represents a conservation equation of the different species (ligands, receptors, and bonds). The k_r and k_f are functions of bond length:

$$k_r = k_r^0 \exp\left(-(k_s - k_{ts})L^2/2B_z\right) \tag{2}$$

$$k_f = k_f^0 \exp\left(-k_{ts}L^2/2B_z\right) \tag{3}$$

Where k_s is the bond elastic constant; k_{ts} is the bond elastic constant at transient state; B_z is thermal energy; k_r^0 and k_f^0 are the reverse and forward reaction rates at zero load of ligand-receptor pair, respectively; L is the difference between bond length y and equilibrium length λ. During the dynamic interaction process, the bond length of a ligand-receptor pair may vary with particle position and orientation. The receptor-ligand bonds are modeled as springs with spring constant σ and equilibrium length λ, thus the bond forces are described as a function of bond length y. Then, the ligand-receptor interaction forces can be summed on finite element surface through integration over the nanoparticle surface. Equations of bond forces f_L and integrated adhesion forces σ^S on particle surface Γ are given as:

$$f_L = \sigma(y - \lambda) \tag{4}$$

$$\sigma^s \cdot n = \int N_b f_L(X^c) d\Gamma \tag{5}$$

Such adhesion force is coupled with the fluid-structure interaction force in the IFEM formulation. Similar adhesion model has been used by Chang et al. [44] and Dong et al. [45] in the study of white blood cell rolling.

The physical parameters used in the model are listed in Table 1 below.

Besides adhesion forces, the Brownian force acting on to the nanoparticles is also important and is integrated into the IFEM formulation by adding a Brownian force term, which is described in the next section.

III. Nanoparticle Brownian Dynamics

Fundamental theories of Brownian dynamics indicate that random collisions from surrounding liquid molecules impact motion of an immersed small particle[49–51]. The influence of Brownian motion on behaviors of nanoparticles in microfluidic channel and platelets and blood cells in blood flow has been studied extensively[2,52–54]. Patankar et al. [55] have proposed an algorithm for direct numerical simulation of Brownian motion by adding random disturbance in fluids. At microscale, the drag force acting on particles such as blood cells is significantly large (> 50 pN for particle size > 1 μm), thus Brownian motion is neglectable[52]. At nanoscale, Brownian force becomes a dominant force to drive nanoparticle near vascular wall surface, while the drag force acting on a nanoparticle is relatively small. The random forces $\mathbf{R}(t)$ and torque $\mathbf{T}(t)$ acting on a nanoparticle is responsible for Brownian motion and rotation and satisfy the fluctuation-dissipation theorem[56]:

$$\langle \mathbf{R}_i(t) \rangle = 0, \langle \mathbf{T}_i(t) \rangle = 0 \tag{6}$$

$$\left\langle \mathbf{R}_i(t)\mathbf{R}_j(t') \right\rangle = 2k_B T\beta_t \delta_{ij}\delta(t-t')\boldsymbol{\delta}, \left\langle \mathbf{T}_i(t)\mathbf{T}_j(t') \right\rangle = 2k_B T\beta_r \delta_{ij}\delta(t-t')\boldsymbol{\delta} \tag{7}$$

Where $\boldsymbol{\delta}$ is the unit-second order tensor, δ_{ij} is the Kronecker delta, $\delta(t - t')$ is the Dirac delta function, k_BT is thermal energy of system, β_t and β_r are the translational and rotational friction coefficient of nanoparticle, respectively.

The friction coefficient depends on several physical parameters, such as fluid viscosity, size and shape of the nanoparticle. The friction coefficient for spherical-shaped particles can be easily derived from Stokes' law. However, there is no empirical formula available for friction coefficient of particles with complex shapes. We have derived the friction coefficient of non-spherical particles both numerically (put particles at different flow configurations and calculate the drag force through IFEM) and empirically. In literature, there are empirical formulas for friction coefficients for particles of simple shapes and orientations such as oblate or rod-shaped particles[57–60]. In a recent work by Loth[61], a new empirical formula is proposed to calculate friction coefficient for a non-spherical particle. Friction coefficient of rod shaped particles in this work is derived based on Loth[61] and extended with an angle factor to consider arbitrary orientations. When a particle moves along the fluid flow, the relative velocity of the particle can be divided into components in two directions: parallel to flow and perpendicular to flow, as shown in Fig. 2.

The friction coefficient of a rod-shaped particle for an arbitrary orientation is given by [61]:

$$\beta_t = 3\pi\mu d_{eqv} \times (f_{\parallel} \cdot |\cos\theta| + f_{\perp} \cdot |\sin\theta|) \tag{8}$$

$$\beta_r = \pi\mu d^3_{eqv} \tag{9}$$

Where β_t is the friction coefficient for translational motion, β_r is the friction coefficient for rotational motion, μ is the fluid viscosity, d_{eqv} is the diameter of particle volume equivalent sphere, θ is the angle between flow direction and the long axis of the particle, $f_{\parallel}$ and $f_{\perp}$ are Stokes correction factors for a spheroid particle moving parallel and perpendicular to the flow, respectively. These correction factors are expressed as [61]:

$$f_{\parallel} = \left(\frac{4}{5} + \frac{\gamma}{5}\right)\gamma^{-1/3} \tag{10}$$

$$f_{\perp} = \left(\frac{3}{5} + \frac{2\gamma}{5}\right)\gamma^{-1/3} \tag{11}$$

Where γ is the aspect ratio of the spheroid particle. The velocity of a particle moving under a deterministic force in a fluid with velocity $\mathbf{V}_f$ is given by:

$$\mathbf{V}_s = \left(\frac{\mathbf{F}_{\text{det}}}{\beta_t} + \mathbf{V}_f\right)(1 - e^{-\frac{\beta_t}{m}t}) \tag{12}$$

Where $\mathbf{F}_{\text{det}}$ is the total deterministic force acting on the nanoparticle (including Brownian force, adhesion force, etc.), $\mathbf{V}_s$ and $\mathbf{V}_f$ are the solid and fluid velocity vectors, respectively. For a time step (usually ~1μs) much greater than characteristic time constant m/β_t (~10 ns), the nanoparticle moves with a terminal velocity, thus Eq. (12) reduces to:

$$\mathbf{V}_s = \frac{\mathbf{F}_{\text{det}}}{\beta_t} + \mathbf{V}_f \tag{13}$$

Eq. 13 actually describes that the deterministic force acting on a particle is balanced by the drag force from the fluid. This is reasonable since the mass of a nanoparticle is so small that inertia effect can be neglected. This terminal velocity is then use to update the nanoparticle position in translational direction. Similarly, the angular velocity of a nanoparticle can be obtained through:

$$\omega_s = \frac{T_{\text{det}}}{\beta_r} + \omega_f \tag{14}$$

Where ω_f is the angular velocity due to fluid flow. Combining the translational and angular velocities, particle nodal positions are updated based on its distance from the particle center as:

$$\mathbf{v}_i = \mathbf{V}_s + \omega_s \times \mathbf{r}_i \tag{15}$$

The fluid flow in our simulation is assumed to be an incompressible viscous fluid governed by the Navier–Stokes equations:

$$\rho\left(\frac{\partial \mathbf{v}_f}{\partial t} + \mathbf{v}_f \cdot \nabla \mathbf{v}_f\right) = -\nabla p + \mu \nabla^2 \mathbf{v}_f \tag{16}$$

$$\nabla \cdot \mathbf{v}_f = 0 \tag{17}$$

It should be noticed that $\mathbf{v}_f$ is the fluid velocity in the fluid main, while $\mathbf{V}_f$ is the fluid velocity interpolated onto the solid domain. The Navier-Stokes equations are solved through finite element method. To reduce numerical oscillations, the velocity test function is employed along with stabilization parameters. Using integration by parts and the divergence theorem, the Patrov-Galarkin weak form is obtained. Then, the nonlinear system is solved using the Newton-Raphson method. Moreover, Generalized Minimum Residual (GMRES) iterative algorithm is employed to improve computation efficiency and to compute residuals based on matrix-free techniques[62]. Details of the implementation can also be referred to Zhang et. al. and Liu et. al[36–38,63].

IV. Simulation Results

There are numerous physical factors that impact nanoparticle interaction with a surface under shear flow, such as particle-wall distance, particle shape, shear rate etc. In particular, the influences of particle shape and ligand density on adhesion will be the focus of this paper. The mesh used and fluid channel dimensions are listed in the Appendix.

a. Influence of Nanoparticle Shape on Adhesion Kinetics

To test the influence of nanoparticle shape on adhesion kinetics, two nanoparticles of different shapes, spherical and non–spherical, but of the same volume are considered. The length of the rod shaped particle considered is 1000 nm with an aspect ratio of 5. The diameter of spherical particle is 380 nm. Such constant volume consideration helps answer an important question for nanomedicine application: given the same drug load capacity, does nanorod or nanosphere bind better? The simulations are carried over a channel of 5 μm long and 2 μm high. In the simulation, a spherical particle and a rod-shaped particle are initially positioned with their centers 600 nm above a receptor-coated surface, as shown in Fig. 3.

A shear velocity is applied at the top of channel to generate a shear rate of $8.0 s^{-1}$. Nanoparticles are allowed to move freely through the channel under the influence of shear flow and Brownian forces. For a typical simulation demonstrated in Fig. 3, the spherical particle fails to make any contact with the vessel wall while it travels through the channel. Under the given velocity and channel length, Brownian diffusion is not large enough to make the spherical particle to reach close enough to the wall surface to initialize bonding. Compared to nanospheres, nanorods make contact and adhere to vessel wall much more frequently. Due to its non-spherical shape, rod-shaped particle exhibits tumbling motion while flowing through the channel. Due to the tumbling motion, a nanorod usually contacts with the receptor coated wall with bonds formed at the long axis end first. Such initial contact is followed by nanoparticle rotation along the contact end and steadily growing

adhesion force, which make it firmly adhere to the vessel wall and settle down at equilibrium state with full contact. The simulation results visualize typical trajectories of a nanosphere and a nanorod, which illustrate different dynamic adhesion processes. A more quantitative description of the adhesion process will be presented in later sections.

One question that might arise up to this point is the existence of such near wall particle tumbling motion. In literature, tumbling of non-spherical particles near a wall surface has been reported in a few studies[35,64,65]. The combined effects of shear flow and Brownian rotation is found to enhance rotation of nanorods[66,67]. In this paper, we have discovered the contribution of nanoparticle tumbling motion toward enhanced contact and binding to vascular wall.

b. Influence of Ligand Density on Adhesion Kinetics

Besides shape, ligand density also largely influences nanoparticle adhesion kinetics. To investigate the effect of ligand density on nanoparticle adhesion kinetics, the deposition process of two nanorods is compared under the same physical flow condition.

In this simulation, a shear rate of $8.0s^{-1}$ is generated within the channel. Nanorods are coated with a ligand density of $410\mu m^{-2}$ and $3400\mu m^{-2}$, respectively. The corresponding numbers of ligands on each particle are 15 and 120, respectively. The significance of ligand density is that larger density results in stronger/faster bond formation. As shown in Fig. 4, a nanorod with low ligand density contacts with the wall surface at its end during tumbling motion, but still wash away due to weak adhesion force. The limited numbers of ligands on the surface are unable to hold the nanoparticle at the contact site. In comparison, a nanorod with high ligand density firmly adheres upon initial contact as a result of multivalent bond formation. Therefore, the large number of bond sites ensures firm adhesion of nanorod at the contact site.

c. Trajectories of multiple nanoparticles

Nanorods are expected to have a higher probability to contact with the wall surface than their spherical counter parts because of the tumbling motion. To test this hypothesis quantitively, trajectories of spherical and non-spherical nanoparticles under the same flow condition are compared. The simulations are carried over a channel with a length of 12 μm and a height of 1.5 μm under a shear rate of $8.0s^{-1}$.

To illustrate the fluctuations of nanoparticle-wall distance, minimum distance between the nanoparticle and the wall surface is recorded over time, as illustrated in Fig. 5. Such trajectory indicates the contact-path of a nanoparticle when it flows through the channel. This determines how close the nanoparticle travels near the wall surface, which is one of the dominant factors for nanoparticle binding.

In a series of runs, a nanosphere and a nanorod are placed initially 650 nm above the wall surface and then released to move freely. The trajectories of nanorod and nanosphere in twenty independent simulations are plotted in Fig. 6A. The simulation result elucidates that a nanorod has larger fluctuations in trajectories due to its tumbling motion, thus has more contact/adhesion events compared to that of a nanosphere, as shown in Fig. 6B. Moreover, out of the twenty trials, ten nanorods are deposited while only three nanospheres are deposited. The probability of a spherical particle to contact with wall surface is purely determined by limited Brownian diffusion; while in case of nanorod, probability of contact is enhanced by tumbling motion. This result supports the hypothesis that nanorod has higher contact probability than the nanosphere for given physical condition.

d. Binding probability of nanoparticles

The numerical method developed in previous sections is a rigorous way to model the full transportation and adhesion dynamics of arbitrarily-shaped nanoparticles. However, to model the adhesion of larger amounts of nanoparticles, it is computationally cost-effective and more convenient to derive a binding probability for nanoparticles under various configurations. The binding probability is the probability of a nanoparticle located within a certain distance from the wall surface to bind with the vascular wall. Binding probability directly determines how many nanoparticles will actually bind to the surface among all nanoparticles present within the fluid channel considered.

It should be noted that only nanoparticles are considered through out this paper. Blood cells have been observed to influence the dispersion rate of nanoparticles. However, the focus of this paper is to characterize the influence of particle shape on its binding property. It is known that to initiate bond formation, nanoparticles must stay very close to the wall surface, inside a near-wall region known as cell free layer (CFL)[68], as shown in Fig. 7. The red blood cells flow with relatively higher velocity in the core region of vessel, leaving a pure plasma region with lower velocity close to vessel wall. The existence of CFL makes it reasonable to only consider nanoparticles in the deposition process. The thickness of the cell free layer is found to be varying from 2–5 μm, independent of vessel size for vessels with diameter above 20 μm [69–71]. This suggests that binding probabilities of nanoparticles should be studied for a range of CFL thicknesses.

This section focuses on studying the effect of two parameters, shear rate and CFL thickness, on nanoparticle binding probability. To ensure consistency and to study sole effect of mentioned parameters among all the cases, the rest of the parameters are kept constant. For example, the value of ligand density is assumed to be sufficiently high to guarantee firm adhesion of nanoparticles (adhesion force typically varies between 1 pN – 100 pN, while dislodging forces are limited around 0.01 pN). Moreover, in a recent study, it has been shown that once a nanoparticle tethers to the receptor coated surface, it is unlikely to get detached under hydrodynamics force[72]. As a consequence, this section focuses on determining binding probability of nanoparticles rather than dissociation probability. The simulation parameters are listed in Table. 1, unless otherwise noted. The diameter and length of nanorod is 200 nm and 1000 nm, respectively. The diameter of nanosphere is 380 nm.

The simulation begins with randomly assigned initial positions of nanoparticle at the channel inlet. Various shear velocities are applied at the top of the channel to generate different shear rates. The nanoparticle transport is simulated by the Brownian adhesion dynamics model. To ensure statistical accuracy, binding probability is evaluated based on the results of 200 independent trials. The number of bonded nanoparticles is counted and normalized by the total number of nanoparticles to obtain the binding probability for a given CFL thickness under a given flow condition.

Binding probability of nanoparticles as a function of CFL thickness is plotted in Fig. 8 for two different shear rates, 10 s^{-1} and 2 s^{-1}, respectively. The nanorods show significantly higher adhesion probability than nanospheres at both shear rates. Fig. 8A shows the binding probability of nanoparticles under a shear rate of 10 s^{-1}. As the CFL thickness increases, binding probability of nanoparticle decreases. Due to limited diffusion length, the binding probability of a nanosphere decreases almost linearly with CFL thickness, except for low CFL thickness of 1.5 μm. At 1.5 μm CFL thickness, the size of nanoparticle becomes comparable to the thickness size, thus results in higher deposition probability. In comparison, the binding probability of nanorod decreases almost quadratically with CFL thickness, mainly due to the tumbling motion. In particular, a nanorod has significantly higher binding probability than nanosphere at small CFL thicknesses. As shear rate

decreases, binding probabilities for both particles increase. At a shear rate of 10 s^{-1} and CFL thickness of 1.5 μm, the binding probability of the nanorod is around 2.5 times of that for the nanosphere. Less difference in binding probability between nanorod and nanosphere is observed at a shear rate of $2s^{-1}$, as shown in Fig. 8B. At lower shear rates, Brownian motion becomes a dominant factor, thus reduces the contribution from tumbling motion.

Besides shape, the effect of nanoparticle aspect ratio is investigated. Nanorods of two aspect ratios (5 and 10) are considered in the study and compared with nanospheres. The binding probability of nanoparticles under different shear rates is plotted in Fig. 9. A CFL thickness of 5 μm is used. It is found that nanoparticle with higher aspect ratio has higher binding probability than that of lower aspect ratio or spherical nanoparticles. The binding probabilities for nanorods are proportional to the aspect ratio with a scaling factor of around 1.6 in a range of shear rates. The simulation result also elucidates that increase in shear rates reduces binding probability of nanoparticles, but the degree of reduction of binding probability varies with different nanoparticles. Binding probability of nanosphere drops largely with increase in shear rate. While that of nanorods drops only marginally with increase in shear rate. This result clearly demonstrates advantage of nanorod over nanosphere in terms of binding probability over a range of shear rates.

V. Conclusions

In summary, the adhesion kinetics of non-spherical nanoparticles is studied for the first time with hydrodynamics coupled with Brownian dynamics. The adhesion kinetics of nanoparticles is found to be influenced by the local flow shear rate, shape, and ligand density of the nanoparticle. While we focus on the rod-shaped nanoparticles, the method developed in this paper is applicable to adhesion dynamics of arbitrarily-shaped nanoparticles. Binding probabilities of nanorods and nanospheres are determined for a range of cell-free layer thicknesses. It is found that nanorod has considerably higher binding probability compared to nanosphere under the same flow condition, mainly due to the tumbling motion. Moreover, with increased shear rate, larger difference in adhesion probability between nanorod and nanosphere is found. The modeling results can be used to optimize the design of shape and size of nanoparticle for desired nanomedicine function, and might eventually help shorten nano-carriers design cycles.

In the future, a more comprehensive model will be developed to include blood cells into the consideration, since cell-particle interaction might influence the nanoparticle dispersion. Such a model can be used to calculate the dispersion coefficient, a parameter governing particles margination from main stream toward wall surface. The dispersion rate will eventually be combined with the deposition rate at near wall region to predict targeted drug delivery efficiency.

Supplementary Material

Refer to Web version on PubMed Central for supplementary material.

Acknowledgments

This work is supported by the National Science Foundation (CBET-0955214) and National Institute of Health (EB009786) to Y.L, the Department of the Army (W81XWH-BAA08) and Moncrief Foundation to W.H and J.G.

References

1. Chauvierre C, Labarre D, Couvreur P, Vauthier C. Novel polysaccharide-decorated poly(isobutyl cyanoacrylate) nanoparticles. Pharmaceutical Research. 2003; 20(11):1786–1793. [PubMed: 14661923]
2. Longest PW, Kleinstreuer C. Comparison of blood particle deposition models for non-parallel flow domains. Journal of Biomechanics. 2003; 36(3):421–430. [PubMed: 12594990]
3. Farokhzad OC, Langer R. Nanomedicine: Developing smarter therapeutic and diagnostic modalities. Advanced Drug Delivery Reviews. 2006; 58(14):1456–1459. [PubMed: 17070960]
4. Mathiowitz E, et al. Biologically erodable microsphere as potential oral drug delivery system. Nature. 1997; 386(6623):410–414. [PubMed: 9121559]
5. Nasongkla N, et al. Multifunctional polymeric micelles as cancer-targeted, mri-ultrasensitive drug delivery systems. Nano Letters. 2006; 6(11):2427–2430. [PubMed: 17090068]
6. Peppas NA. Intelligent biomaterials as pharmaceutical carriers in microfabricated and nanoscale devices. Mrs Bulletin. 2006; 31(11):888–893.
7. Roney C, et al. Targeted nanoparticles for drug delivery through the blood-brain barrier for alzheimer's disease. Journal of Controlled Release. 2005; 108(2–3):193–214. [PubMed: 16246446]
8. Shah P. Use of nanotechnologies for drug delivery. Mrs Bulletin. 2006; 31(11):894–899.
9. Sukhorukov GB, Mohwald H. Multifunctional cargo systems for biotechnology. Trends in Biotechnology. 2007; 25(3):93–98. [PubMed: 17207546]
10. Liu Y, Lu WL, Zhang Q. Recent advances in liposomes and nanoparticles as drug carriers for drug delivery. Zhongguo Yi Xue Ke Xue Yuan Xue Bao. 2006; 28(4):583–9. [PubMed: 16995319]
11. Sharma G, Anabousi S, Ehrhardt C, Ravi Kumar MN. Liposomes as targeted drug delivery systems in the treatment of breast cancer. J Drug Target. 2006; 14(5):301–10. [PubMed: 16882550]
12. Maysinger D, Lovric J, Eisenberg A, Savic R. Fate of micelles and quantum dots in cells. Eur J Pharm Biopharm. 2007; 65(3):270–81. [PubMed: 17027243]
13. Sutton D, Nasongkla N, Blanco E, Gao J. Functionalized micellar systems for cancer targeted drug delivery. Pharm Res. 2007; 24(6):1029–46. [PubMed: 17385025]
14. Torchilin VP. Targeted polymeric micelles for delivery of poorly soluble drugs. Cell Mol Life Sci. 2004; 61(19–20):2549–59. [PubMed: 15526161]
15. Gao X, Yang L, Petros JA, Marshall FF, Simons JW, Nie S. In vivo molecular and cellular imaging with quantum dots. Curr Opin Biotechnol. 2005; 16(1):63–72. [PubMed: 15722017]
16. Smith AM, Ruan G, Rhyner MN, Nie S. Engineering luminescent quantum dots for in vivo molecular and cellular imaging. Ann Biomed Eng. 2006; 34(1):3–14. [PubMed: 16450199]
17. Koenig S, Chechik V. Shell cross-linked au nanoparticles. Langmuir. 2006; 22(11):5168–73. [PubMed: 16700609]
18. Lou X, Wang C, He L. Core-shell au nanoparticle formation with DNA-polymer hybrid coatings using aqueous atrp. Biomacromolecules. 2007; 8(5):1385–90. [PubMed: 17465524]
19. Yang Y, Nogami M, Shi J, Ruan M. Template guided self-assembling two-dimensional array of au@sio2 core-shell nanoparticles for room-temperature single electron transistors. J Nanosci Nanotechnol. 2005; 5(2):179–83. [PubMed: 15853133]
20. Cheng Y, Gao Y, Rao T, Li Y, Xu T. Dendrimer-based prodrugs: Design, synthesis, screening and biological evaluation. Comb Chem High Throughput Screen. 2007; 10(5):336–49. [PubMed: 17896929]
21. Duncan R, Izzo L. Dendrimer biocompatibility and toxicity. Adv Drug Deliv Rev. 2005; 57(15): 2215–37. [PubMed: 16297497]
22. Najlah M, D'emanuele A. Crossing cellular barriers using dendrimer nanotechnologies. Curr Opin Pharmacol. 2006; 6(5):522–7. [PubMed: 16890022]
23. Geng Y, Dalhaimer P, Cai SS, Tsai R, Tewari M, Minko T, Discher DE. Shape effects of filaments versus spherical particles in flow and drug delivery. Nature Nanotechnology. 2007; 2(4):249–255.
24. Liu Z, et al. In vivo biodistribution and highly efficient tumour targeting of carbon nanotubes in mice. Nature Nanotechnology. 2007; 2(1):47–52.

25. Park JH, Von Maltzahn G, Zhang LL, Schwartz MP, Ruoslahti E, Bhatia SN, Sailor MJ. Magnetic iron oxide nanoworms for tumor targeting and imaging. Advanced Materials. 2008; 20(9):1630.
26. Galbraith CG, Sheetz MP. Forces on adhesive contacts affect cell function. Current Opinion in Cell Biology. 1998; 10(5):566–571. [PubMed: 9818165]
27. Decuzzi P, Ferrari M. The adhesive strength of non-spherical particles mediated by specific interactions. Biomaterials. 2006; 27(30):5307–14. [PubMed: 16797691]
28. Decuzzi P, Lee S, Bhushan B, Ferrari M. A theoretical model for the margination of particles within blood vessels. Annals of Biomedical Engineering. 2005; 33(2):179–190. [PubMed: 15771271]
29. Decuzzi P, Lee S, Decuzzi M, Ferrari M. Adhesion of microfabricated particles on vascular endothelium: A parametric analysis. Annals of Biomedical Engineering. 2004; 32(6):793–802. [PubMed: 15255210]
30. Winter WT, Welland ME. Dielectrophoresis of non-spherical particles. Journal of Physics D-Applied Physics. 2009; 42(4)
31. Liu YL, Chung JH, Liu WK, Ruoff RS. Dielectrophoretic assembly of nanowires. Journal of Physical Chemistry B. 2006; 110(29):14098–14106.
32. Liu YL, et al. Manipulation of nanoparticles and biomolecules by electric field and surface tension. Computer Methods in Applied Mechanics and Engineering. 2008; 197(25–28):2156–2172.
33. Djohari H, Dormidontova EE. Kinetics of nanoparticle targeting by dissipative particle dynamics simulations. Biomacromolecules. 2009; 10(11):3089–3097. [PubMed: 19894765]
34. Mody NA, Lomakin O, Doggett TA, Diacovo TG, King MR. Mechanics of transient platelet adhesion to von willebrand factor under flow. Biophysical Journal. 2005; 88(2):1432–1443. [PubMed: 15533923]
35. Mody NA, King MR. Three-dimensional simulations of a platelet-shaped spheroid near a wall in shear flow. Physics of Fluids. 2005; 17(11)
36. Zhang L, Gerstenberger A, Wang XD, Liu WK. Immersed finite element method. Computer Methods in Applied Mechanics and Engineering. 2004; 193(21–22):2051–2067.
37. Liu WK, et al. Immersed finite element method and its applications to biological systems. Computer Methods in Applied Mechanics and Engineering. 2006; 195(13–16):1722–1749. [PubMed: 20200602]
38. Liu WK, Kim DW, Tang SQ. Mathematical foundations of the immersed finite element method. Computational Mechanics. 2007; 39(3):211–222.
39. Lee TR, Chang YS, Choi JB, Kim DW, Liu WK, Kim YJ. Immersed finite element method for rigid body motions in the incompressible navier-stokes flow. Computer Methods in Applied Mechanics and Engineering. 2008; 197(25–28):2305–2316.
40. Liu YL, Liu WK. Rheology of red blood cell aggregation by computer simulation. Journal of Computational Physics. 2006; 220(1):139–154.
41. Liu YL, Zhang L, Wang XD, Liu WK. Coupling of navier-stokes equations with protein molecular dynamics and its application to hemodynamics. International Journal for Numerical Methods in Fluids. 2004; 46(12):1237–1252.
42. Lutters BCH, Leeuwenburgh MA, Appeldoorn CCM, Molenaar TJM, Van Berkel TJC, Biessen EAL. Blocking endothelial adhesion molecules: A potential therapeutic strategy to combat atherogenesis. Current Opinion in Lipidology. 2004; 15(5):545–552. [PubMed: 15361790]
43. Dembo M, Torney DC, Saxman K, Hammer D. The reaction-limited kinetics of membrane-to-surface adhesion and detachment. Proceedings of the Royal Society of London Series B-Biological Sciences. 1988; 234(1274):55–83.
44. Chang KC, Tees DFJ, Hammer DA. The state diagram for cell adhesion under flow: Leukocyte rolling and firm adhesion. Proceedings of the National Academy of Sciences of the United States of America. 2000; 97(21):11262–11267. [PubMed: 11005837]
45. Dong C, Cao J, Struble EJ, Lipowsky HW. Mechanics of leukocyte deformation and adhesion to endothelium in shear flow. Annals of Biomedical Engineering. 1999; 27(3):298–312. [PubMed: 10374723]

46. Lawrence MB, Springer TA. Leukocytes roll on a selectin at physiological flow-rates - distinction from and prerequisite for adhesion through integrins. Cell. 1991; 65(5):859–873. [PubMed: 1710173]
47. Bell GI, Dembo M, Bongrand P. Cell-adhesion - competition between nonspecific repulsion and specific bonding. Biophysical Journal. 1984; 45(6):1051–1064. [PubMed: 6743742]
48. Bell GI. Models for specific adhesion of cells to cells. Science. 1978; 200(4342):618–627. [PubMed: 347575]
49. Einstein, A. Investigations on the theory of brownian movement. New York: Dover; 1956.
50. Ermak DL, Mccammon JA. Brownian dynamics with hydrodynamic interactions. Journal of Chemical Physics. 1978; 69(4):1352–1360.
51. Li A, Ahmadi G. Dispersion and deposition of spherical-particles from point sources in a turbulent channel flow. Aerosol Science and Technology. 1992; 16(4):209–226.
52. Mody NA, King MR. Influence of brownian motion on blood platelet flow behavior and adhesive dynamics near a planar wall. Langmuir. 2007; 23(11):6321–8. [PubMed: 17417890]
53. Gentile F, Ferrari M, Decuzzi P. The transport of nanoparticles in blood vessels: The effect of vessel permeability and blood rheology. Annals of Biomedical Engineering. 2008; 36(2):254–261. [PubMed: 18172768]
54. Lee TR, Chang YS, Choi JB, Liu WK, Kim YJ. Numerical simulation of a nanoparticle focusing lens in a microfluidic channel by using immersed finite element method. Journal of Nanoscience and Nanotechnology. 2009; 9(12):7407–7411. [PubMed: 19908798]
55. Sharma N, Patankar NA. Direct numerical simulation of the brownian motion of particles by using fluctuating hydrodynamic equations. Journal of Computational Physics. 2004; 201(2):466–486.
56. Mori N, Kumagae M, Nakamura K. Brownian dynamics simulation for suspensions of oblong-particles under shear flow. Rheologica Acta. 1998; 37(2):151–157.
57. Inthavong K, Wen H, Tian ZF, Tu JY. Numerical study of fibre deposition in a human nasal cavity. Journal of Aerosol Science. 2008; 39(3):253–265.
58. Haider A, Levenspiel O. Drag coefficient and terminal velocity of spherical and nonspherical particles. Powder Technology. 1989; 58(1):63–70.
59. Tran-Cong S, Gay M, Michaelides EE. Drag coefficients of irregularly shaped particles. Powder Technology. 2004; 139(1):21–32.
60. Dimaki M, Boggild P. Dielectrophoresis of carbon nanotubes using microelectrodes: A numerical study. Nanotechnology. 2004; 15(8):1095–1102.
61. Loth E. Drag of non-spherical solid particles of regular and irregular shape. Powder Technology. 2008; 182(3):342–353.
62. Saad Y, Schultz MH. Gmres - a generalized minimal residual algorithm for solving nonsymmetric linear-systems. Siam Journal on Scientific and Statistical Computing. 1986; 7(3):856–869.
63. Liu Y, Liu WK, Belytschko T, Patankar N, To AC, Kopacz A, Chung JH. Immersed electrokinetic finite element method. International Journal for Numerical Methods in Engineering. 2007; 71(4): 379–405.
64. Pozrikidis C. Flipping of an adherent blood platelet over a substrate. Journal of Fluid Mechanics. 2006; 568:161–172.
65. Gavze E, Shapiro M. Particles in a shear flow near a solid wall: Effect of nonsphericity on forces and velocities. International Journal of Multiphase Flow. 1997; 23(1):155–182.
66. Naess SN, Elgsaeter A. Transport properties of non-spherical nanoparticles studied by brownian dynamics: Theory and numerical simulations. Energy. 2005; 30(6):831–844.
67. Forest MG, Heidenreich S, Hess S, Yang XF, Zhou RH. Robustness of pulsating jet-like layers in sheared nano-rod dispersions. Journal of Non-Newtonian Fluid Mechanics. 2008; 155(3):130–145.
68. Zhang JF, Johnson PC, Popel AS. Effects of erythrocyte deformability and aggregation on the cell free layer and apparent viscosity of microscopic blood flows. Microvascular Research. 2009; 77(3):265–272. [PubMed: 19323969]
69. Woodcock JP. Physical-properties of blood and their influence on blood-flow measurement. Reports on Progress in Physics. 1976; 39(1):65–127.

70. Bayliss LE. The axial drift of the red cells when blood flows in a narrow tube. J Physiol. 1959; 149:593–613. [PubMed: 13797830]

71. Taylor M. The flow of blood in narrow tubes. Ii. The axial stream and its formation, as determined by changes in optical density. Aust J Exp Biol Med Sci. 1955; 33(1):1–15. [PubMed: 14389168]

72. Haun JB, Hammer DA. Quantifying nanoparticle adhesion mediated by specific molecular interactions. Langmuir. 2008; 24(16):8821–8832. [PubMed: 18630976]

Appendix

In our simulations, two independent sets of meshes are used for solid particles and fluid domain, as shown in the Fig A1. Each nanorod consists of 1404 nodes and 5996 elements. Each nanosphere consists of 3213 nodes and 14286 elements. The fluid mesh has 2930 nodes and 8325 elements. The dimensions of the nanoparticles and fluid domain are shown in Fig. A1. A time step of 0.1 ms is used in the simulation.

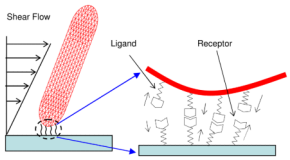

Fig. 1.
Model of ligand-receptor binding kinetics between ligand-coated nanoparticle surface and receptor coated vascular wall surface.

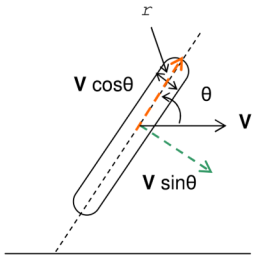

Fig. 2.
Illustration of friction coefficient measurement of arbitrarily orientated nanorod

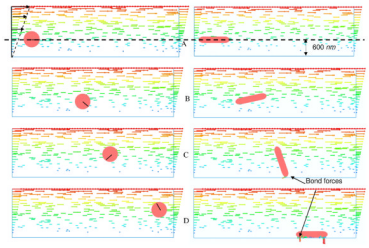

Fig. 3.

Shape dependent adhesion dynamics. The left column shows a spherical particle washed away without contact with surface; the right column shows a nanorod tumbles and gets deposited. A, B, C, D are at times t=0 s, 0.25 s, 0.5s, and 0.75 s, respectively. The line labeled on the spherical particle indicates its rotation. The vectors in fluid domain indicate flow field and arrows indicate magnitude and direction of bonding forces.

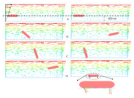

Fig. 4.
Influence of ligand density on adhesion. The left column and right column has a nanorod with low and high ligand coating densities respectively; A, B, C, D are at t=0 s, 0.25 s, 0.5s, and 0.75 s. The vectors in fluid domain indicate flow field and arrows indicate magnitude and direction of bonding forces.

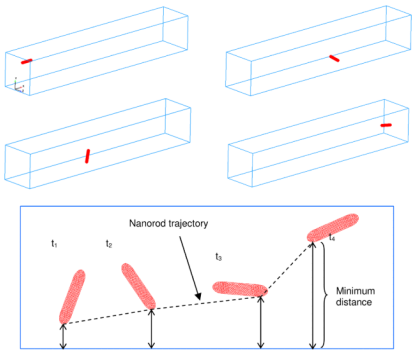

Fig. 5.

Illustration of particle trajectory calculation. The nanorod trajectory is defined as the minimum distance between the nanorod surface and the wall surface at any given time. Center of mass of the nanorod is not used in calculation because it doesn't reflect true minimum distance which actually dictates the binding event.

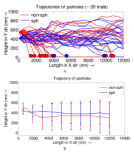

Fig. 6.

Trajectories of a nanorod and a nanosphere. (a) Trajectories of 20 trials of nanorod and nanosphere, where red spots indicate adhesion of nanorods and blue spots indicate adhesion of nanospheres at that location; (b) Mean trajectory of 20 trials of nanorod and nanosphere with standard deviation shown as vertical bar.

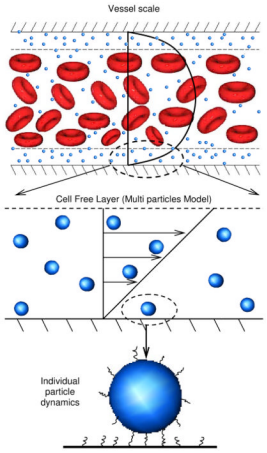

Fig. 7.
Multiscale model of the nanoparticle targeted delivery process.

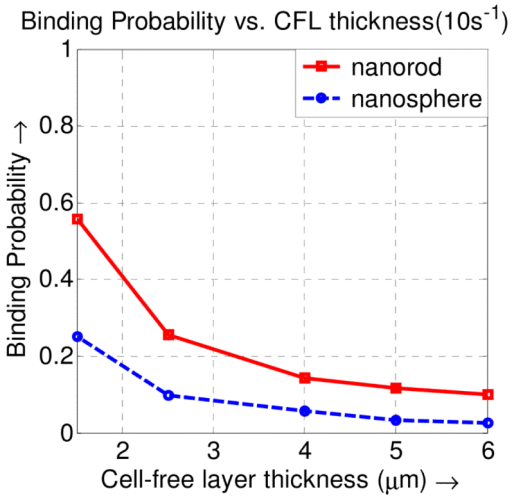

A

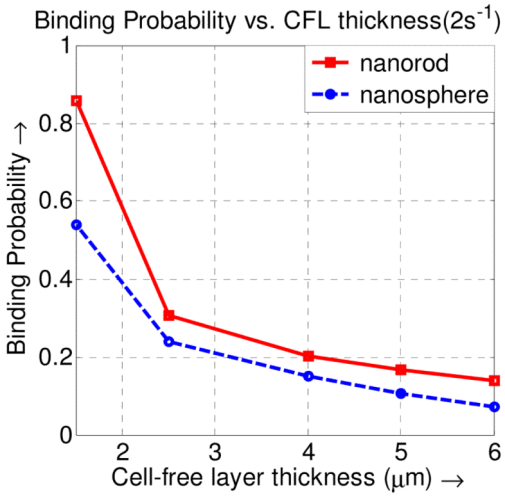

B

Fig. 8.

Binding probabilities of a nanorod and a nanospheres at various cell-free layer thicknesses. (A–B) Binding probability of nanorod and nanosphere at shear rates of $10s^{-1}$ and $2s^{-1}$, respectively.

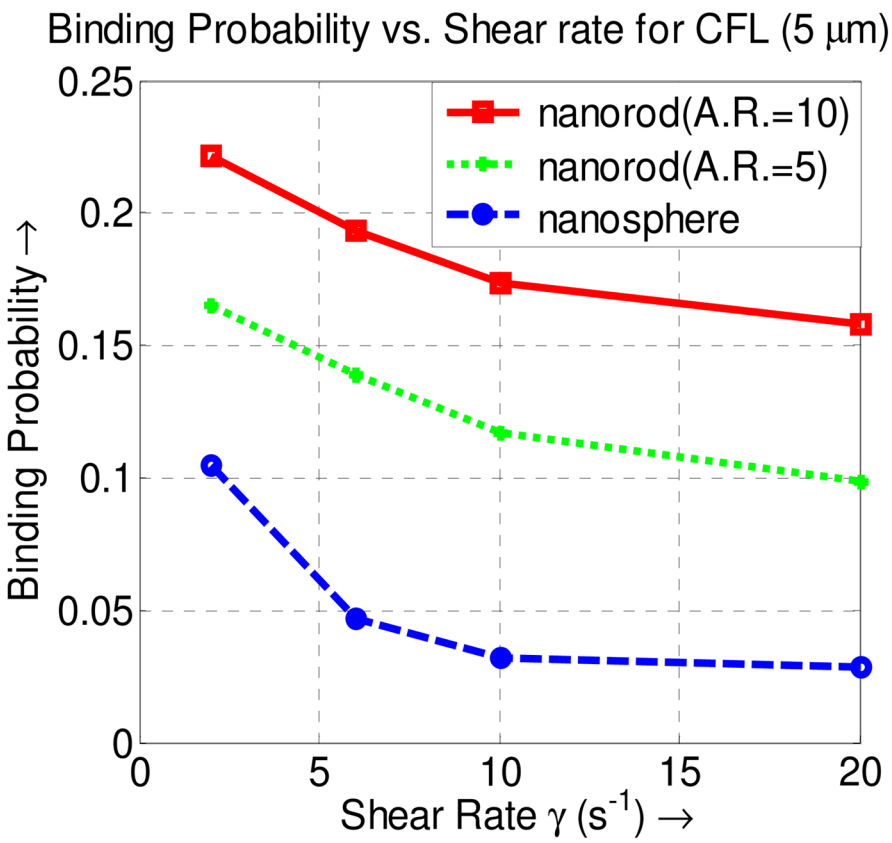

Fig. 9.
Binding probabilities of nanosphere and nanorods of two different aspect ratios for CFL thickness of 5 μm.

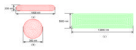

Fig. A1.
Meshes used in the simulation (a) Nanorod (b) Nanosphere (c) fluid channel.

Table 1

List of physical parameters used in the nanoparticle adhesion kinetics model

Definition	Symbol	Value	Reference
Ligand Density	N_l	2.0×10^{10} (sites/cm^2)	Lawrence and Springer (1991)[46]
Receptor Density	N_r	$2.0 – 5.0 \times 10^{10}$ (sites/cm^2)	Bell et al. (1984)[47]
Reverse reaction rate	k_r^0	0.5 (1/s)	Bell (1978)[48]
Forward reaction rate	k_f^0	1.0×10^{-9} (cm^2/s)	Bell (1978) [48]
Equilibrium bond length	λ	20 nm	Bell (1978)[48]
Static bond spring constant	σ	0.5 (dyne/cm)	Dembo et al. (1988)[43]
Transient bond elastic constant	k_{ts}	0.48 (dyne/cm)	Dembo et al. (1988)[43]
Thermal Energy	B_z	4.0×10^{-14} (erg)	Dembo et al. (1988)[43]
Fluid viscosity	μ	0.01 (g/cm-s)	-